



Quantum approach to the thermalization of the toppling pencil interacting with a finite bathSreeja Loho Choudhury *Max-Planck-Institut für Physik Komplexer Systeme, Nöthnitzer Straße 38, D-01187 Dresden, Germany
and Institut für Theoretische Physik, Technische Universität Dresden, D-01062 Dresden, Germany*Frank Grossmann **Institut für Theoretische Physik, Technische Universität Dresden, D-01062 Dresden, Germany*

(Received 18 November 2021; accepted 21 January 2022; published 2 February 2022)

We investigate the longstanding problem of thermalization of quantum systems coupled to an environment by focusing on a bistable quartic oscillator interacting with a finite number of harmonic oscillators. In order to overcome the exponential wall that one usually encounters in grid-based approaches to solve the time-dependent Schrödinger equation of the extended system, methods based on the time-dependent variational principle are best suited. Here we will apply the method of coupled coherent states [D. V. Shalashilin and M. S. Child, *J. Chem. Phys.* **113**, 10028 (2000)]. By investigating the dynamics of an initial wave function on top of the barrier of the double well, it will be shown that only a handful of oscillators with suitably chosen frequencies, starting in their ground states, is enough to drive the bistable system close to its uncoupled ground state. The long-time average of the double-well energy is found to be a monotonously decaying function of the number of environmental oscillators in the parameter range that was numerically accessible.

DOI: [10.1103/PhysRevA.105.022201](https://doi.org/10.1103/PhysRevA.105.022201)**I. INTRODUCTION**

Ever since the pioneering works of Fermi, Pasta, Ulam, and Tsingou (FPUT) [1,2], the puzzle of energy exchange between subsystems, eventually leading to equilibration and thermalization in closed systems with a finite number of degrees of freedom, has intrigued researchers in the fields of classical [3–11], as well as semiclassical [12,13] and quantum mechanics [3,14–20]. In the quantum context, an important concept is the eigenstate thermalization hypothesis (ETH) [21,22]. Whereas thermalization in classical systems is closely related to the presence of chaos and ergodicity, the ETH can be regarded, very broadly, as the quantum manifestation of such ergodic behavior. The principal philosophy underlying the ETH, however, is that instead of explaining the ergodicity of a thermodynamic system through the mechanism of dynamical chaos, as done in classical mechanics, one should instead examine the properties of matrix elements of observable quantities in individual energy eigenstates of the system. The eigenstate thermalization hypothesis states that for an arbitrary initial state of the system, the expectation value of any observable (of a subsystem) will ultimately evolve in time to its value predicted by a microcanonical ensemble and thereafter will exhibit only small fluctuations around that value.

In classical systems the prerequisite for thermalization is believed to be the (hard) chaoticity of the underlying dynamics [4,5], this fact being one possible reason that by investigating a weakly anharmonic system, FPUT did not succeed in finding thermalization but were surprised by a dynamics that showed pronounced revivals [2]. For dynamical

chaos to appear, the phase space has to be at least three dimensional. The question therefore arises as to whether it is enough to increase the interaction strength between the different degrees of freedom in order to fully develop chaos, or if, in addition, the number of those degrees of freedom has to be increased (possibly all the way to the thermodynamic limit) in order to observe thermalization. In two more recent contributions from the realm of classical mechanics it has been shown by solving Newton's equations for coupled harmonic oscillator systems, comprising a few hundred [7] up to a few thousand degrees of freedom [10] that, for a suitably chosen initial configuration, a (large enough) subsystem may indeed reach thermal equilibrium, without coupling to an (external) thermostat and even without nonlinear interactions (i.e., without chaos). In light of these results, another possible reason that FPUT saw no signs of thermalization is the closeness of their model to the noninteracting case [10].

Although semiclassical approaches may be helpful to tackle such problems [23], this large number of degrees of freedom seems elusive if one is interested in a full quantum description of the process. From this perspective it comes as a relief that also small numbers of degrees of freedom (below 10) can lead to thermalization in long-time dynamics of quantum systems, as shown long ago for spin systems [14] and discussed more recently in the seminal book by Gemmer *et al.* [15] and the article by Reimann [19]. For a more recent reference on spin systems realized in graphene quantum dots, see Ref. [24], and for energy exchange in quantum systems with continuous degrees of freedom, see Ref. [17]. There it is claimed that as little as 10–20 harmonic degrees of freedom are necessary to observe energy loss to the bath without backflow on the observed timescales. In addition, in [16] the thermalization of eight valence electrons inside a

*Corresponding author: frank@physik.tu-dresden.de

small sodium cluster has been investigated quantum mechanically. Furthermore, whereas in [14] it was argued that both integrable as well nonintegrable systems exhibit statistical behavior for long times, in [18] it was pointed out that, in a Bose-Hubbard dynamics, thermalization is only observed if the system starts from a chaotic region of phase space but not if the system is launched from a quasi-integrable region.

In the present contribution, we will investigate the toppling pencil model, studied recently by Dittrich and Pena Martínez (DPM) [11]. In their classical mechanics study, they focused on a particle on top of the barrier in a quartic double well that is coupled to a small (from just one single up to the order of ten and higher) number of harmonic oscillators. It is well known that the transition from integrable to chaotic motion sets in first around the separatrix of the double well's phase space, when the interaction strength with an external sinusoidal field is tuned higher [25]. In the light of the findings in [18], this makes an initial condition starting on top of the double well's barrier an ideal candidate to search for (quick [19]) thermalization under the interaction with a relatively small number of harmonic degrees of freedom, although the interaction with a sinusoidal field is a crude approximation to the interaction with harmonic degrees of freedom, whose dynamics is influenced by "back action" of the system.

In contrast to DPM, in the following we will investigate the system dynamics fully quantum mechanically, making use of the method of coupled coherent states (CCS) introduced by Shalashilin and Child [26]. By being based on an expansion of the total wave function in terms of coherent states (Gaussians), whose initial positions in phase space are chosen randomly, the exponential wall that one usually experiences in grid-based approaches to the quantum dynamics can be overcome or at least pushed to rather larger numbers of degrees of freedom. For a recent review of the CCS and related methods, we refer to [27]. The main focus of the present work is on the question of how many bath degrees will be needed to ensure thermalization and how strong the interaction has to be, and how the speed of thermalization depends on the coupling and/or the number of degrees of freedom. The toppling pencil model setup seems to be ideally suited to answer all those questions.

The manuscript is structured as follows: In Sec. II, we briefly introduce the bistable quartic oscillator toppling pencil model coupled to a harmonic heat bath. In Sec. III the CCS method that will be employed to study the quantum dynamics of the many-particle system will be reviewed. In Sec. IV numerical results for several quantities of interest are presented. These are energy expectation values, autocorrelation functions, as well as reduced densities that allow us to observe the transition of the quartic degree of freedom into some almost stationary state resembling the ground state of the unperturbed problem to a large degree. Some conclusions as well as an outlook are given in the final section. The Appendix contains details for the implementation of the CCS method.

II. QUARTIC DOUBLE WELL COUPLED TO A FINITE HEAT BATH

Our model system is a double well which is bilinearly coupled to a finite number f of harmonic oscillators [11]. A

quartic double well is a bistable system with two symmetry-related minima. It has many physical realizations, one of the most prominent of which is the ammonia molecule, first discussed in the quantum (tunneling) context by Hund as early as 1927 [28]. A solid-state realization of a nonquartic but symmetric double-well potential is given by a suitably parametrized rf-superconducting quantum interference device (SQUID), where the role of the coordinate is played by the flux through the ring [29]. More recently, bistable potentials have been discussed in cold atom physics in connection with Bose-Einstein condensation [30]. In the following we first discuss the bare quartic bistable system before coupling it to a finite heat bath.

A. Quartic double well

The potential of a symmetric quartic oscillator double well with a parabolic barrier around its relative maximum can be written as

$$V_S(x) = -\frac{a}{2}x^2 + \frac{b}{4}x^4, \quad a, b \in \mathbb{R}^+. \quad (1)$$

It has quadratic minima at $x_{\pm} = \pm\sqrt{\frac{a}{b}}$ and a quadratic maximum at $x_0 = 0$ of relative height $E_B = \frac{a^2}{4b}$. The Hamiltonian of the quartic double well is then given by

$$H_S(p_x, x) = \frac{p_x^2}{2m_x} + V_S(x). \quad (2)$$

Its classical dynamics consists of harmonic oscillations with the frequency $\omega = \sqrt{\frac{2a}{m_x}}$ close to the minima at x_{\pm} . These oscillations become increasingly anharmonic as the energy rises towards the top of the barrier. The phase-space portrait of the dynamics contains the prototypical separatrix, shaped like the number 8, as well as a hyperbolic fixed point at $p_x = 0, x = 0$ on that separatrix and two elliptic fixed points at $p_x = 0, x = x_{\pm}$ [31]. If the available energy is higher than the barrier, in the case of the NH_3 molecule, the corresponding motion is referred to as umbrella motion.

For an understanding of the corresponding quantum dynamics, we first calculate the energy spectrum of the quartic double-well potential, using a finite-difference representation of the Laplacian to solve the time-independent Schrödinger equation (TISE):

$$\hat{H}_S \phi_n(x) \equiv \left[-\frac{\hbar^2}{2m_x} \Delta + V_S(x) \right] \phi_n(x) = E_n \phi_n(x). \quad (3)$$

The first few eigenvalues for the parameters $m_x = 1$ and $a = 2, b = 1$ and in units, where $\hbar = 1$, are gathered in Table I. In the numerical work to be shown later, we will use a Gaussian of the form

$$\Psi(x, 0) = \left(\frac{\gamma_x}{\pi} \right)^{1/4} e^{-\frac{\gamma_x}{2} x^2} \quad (4)$$

that is located at the top of the barrier as the initial state. Together with the potential and its first eigenstate it is shown in Fig. 1. The base lines for the two wave functions are at their corresponding energy expectation values, which in the case of the Gaussian is $E_G = \gamma_x/4 - 1/(2\gamma_x) + 3/(16\gamma_x^2)$, leading to $E_G = 0.3$ for a width parameter of $\gamma_x = 2$. Although both

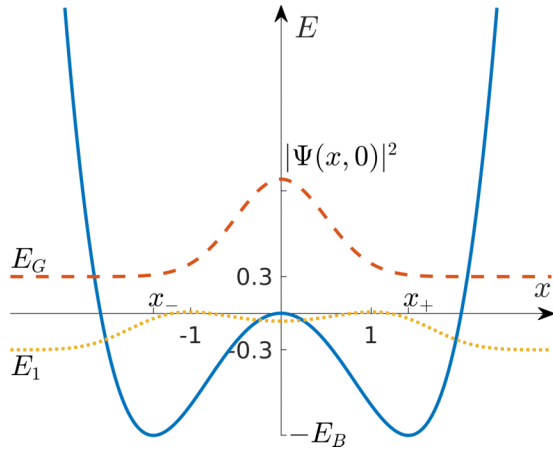


FIG. 1. Quartic double-well potential with parameters $a = 2$, $b = 1$ (solid blue line), leading to $x_{\pm} = \pm\sqrt{2}$. Absolute value squared of the initial Gaussian sitting at the top of the barrier with initial energy $E_G = 0.3$ (dashed red line) and absolute value squared of the ground-state wave function of the quartic double well with ground-state energy $E_1 = -0.30$ (dotted yellow line) are overlaid.

the initial position as well as momentum expectations are zero, due to its finite width, there is a finite energy content in the wave packet. This initial state is the motivation for the naming “toppling pencil”—a pencil balanced tip down on a flat surface, prone to fall over [11].

For symmetry reasons it is obvious that the symmetric initial Gaussian does have zero overlap with the eigenfunctions of odd parity (see Table I). Like the odd ones, also almost all higher even eigenstates (from the fifth eigenstate on) are not taking part in the dynamics. The dynamics of the Gaussian in the bare potential will then be an oscillation with the frequency corresponding to the difference of the first and the third eigenvalue. We stress that this is not the usual tunneling scenario, where a Gaussian is sitting in one of the two wells initially and is then moving to the other well and back with a (usually very small) frequency given by the difference $E_2 - E_1$ of the two lowest eigenvalues. Here we focus on the symmetric initial condition, however, and have chosen the potential parameters such that just the eigenstates with eigenvalues E_1 and E_3 are appreciably populated.

B. Coupling to a finite heat bath

Coupling a double well to a harmonic oscillator heat bath with infinitely many degrees of freedom with continuous

TABLE I. Eigenvalues E_n and squared overlap $|c_n|^2 := |\langle \phi_n | \Psi(0) \rangle|^2$ of eigenstates with the initial Gaussian of Eq. (4) for $\gamma_x = 2$ of the bare quartic double well with $a = 2$, $b = 1$. The grid extension for the finite-difference calculation was $x \in [-4, 4]$ and 256 grid points were sufficient to achieve convergence to within the number of digits given.

	$n = 1$	$n = 2$	$n = 3$	$n = 4$	$n = 5$
E_n	-0.300	0.046	1.23	2.46	3.94
$ c_n ^2$	0.654	0	0.323	0	0.0225

spectral density will lead to decoherence and dissipation in the dynamics. In the case that only the two lowest states of the bistable system play a role, the tunneling rate will be severely influenced by the system bath coupling [32]. A lot of work has been done on that so-called spin-boson model in the '80s of the last century, as documented by the impressive review by Leggett *et al.* [33]. More recently, this model has been studied deeply by different numerical methods, with a focus on correctly mimicking infinite baths by either a discretization in frequency of the harmonic oscillator spectral density or by a correct description of the bath correlation function in the time domain [34]. Furthermore, also the influence of a sinusoidal driving on the tunneling effect in a two-level system has been studied, yielding surprising localization effects [35,36].

Here we are not restricting ourselves to the spin-boson case but will consider the total Hamiltonian to be that of the full bistable system coupled to an environment with a large but finite number of degrees of freedom, given by

$$H(\mathbf{R}, \mathbf{r}) = H_S(\mathbf{R}) + H_E(\mathbf{r}) + H_{SE}(\mathbf{R}, \mathbf{r}), \quad (5)$$

where $\mathbf{R} = (p_x, x)$ denotes the phase-space vector of the central system of interest, whereas $\mathbf{r} = (p_1, p_2, \dots, p_f, y_1, y_2, \dots, y_f)$ denotes the $2f$ -dimensional phase-space vector of all the environmental degrees of freedom. The dynamics of the bare central system of interest (index S) is governed by the Hamiltonian of the quartic double well given in Eq. (2). The environment (index E) consists of f harmonic oscillators, whose Hamiltonian is given by

$$H_E(\mathbf{r}) = \sum_{n=1}^f \left(\frac{p_n^2}{2m} + \frac{m\omega_n^2}{2} y_n^2 \right). \quad (6)$$

The choice of a discrete set of frequencies ω_n , $n = 1, \dots, f$ will be discussed below in the numerical results section. As each oscillator should exert a force on the system, their interaction can be modeled as the position-position coupling,

$$H_{SE}(\mathbf{R}, \mathbf{r}) = -x \sum_{n=1}^f g_n y_n, \quad (7)$$

with coupling constant $g_n = \frac{g}{\sqrt{f}}$, which is renormalized by \sqrt{f} in order to make the results for different number of oscillators comparable. Using linear response theory, this scaling has been derived in [8].

The bilinear coupling does not break the invariance of the total Hamiltonian under a parity transformation (spatial reflection) $P : (\mathbf{R}, \mathbf{r}) \rightarrow (-\mathbf{R}, -\mathbf{r})$. However, it drives the two bistable minima apart from $x_{\pm} = \pm\sqrt{\frac{a}{b}}$ to $x_{\pm} = \pm\sqrt{\frac{1}{b} \left(a + \sum_{n=1}^f \frac{g_n^2}{m\omega_n^2} \right)}$, an effect which is not intended by the coupling to the environment [11,37]. This driving apart can, however, be compensated by including the so-called counterterm proportional to the square of the system coordinate in the potential of the total Hamiltonian (system plus bath) to complete the squares with respect to the dependence on the oscillator coordinates. One thus replaces the total potential by

[11,37,38]

$$\begin{aligned} V_S + V_E + H_{SE} + V_C \\ &= V_S(x) + \sum_{n=1}^f \frac{m\omega_n^2}{2} y_n^2 - x \sum_{n=1}^f g_n y_n + x^2 \sum_{n=1}^f \frac{g_n^2}{2m\omega_n^2} \\ &= V_S(x) + \sum_{n=1}^f \frac{m\omega_n^2}{2} \left(y_n - \frac{g_n}{m\omega_n^2} x \right)^2. \end{aligned} \quad (8)$$

The counterterm,

$$V_C = x^2 \sum_{n=1}^f \frac{g_n^2}{2m\omega_n^2}, \quad (9)$$

now renormalizes the factor a in front of the quadratic term in the system coordinate according to $a \rightarrow a - \sum_{n=1}^f \frac{g_n^2}{m\omega_n^2}$ [39], thus exactly undoing the renormalization (shift of the minima) mentioned above and the minima are at their uncoupled positions, see also Fig. 2 of [11]. In the section on the numerical results, we will display the time evolution of the counterterm V_C . Even more importantly, we will start the bath in its ground state (in the thermodynamic limit $f \rightarrow \infty$ this would correspond to zero temperature) and will focus on the evolution of the system dynamics away from the excited state on top of the barrier. To this end we will need a numerical method that allows us to treat a multitude of degrees of freedom quantum mechanically. The method of our choice is the CCS method to be reviewed in the following.

III. COUPLED COHERENT STATES METHOD

To tackle the quantum dynamics under the many-body Hamiltonian from the previous section, grid-based methods are running into an exponential wall, and we will use a variational approach, based on time-evolving coherent states, that was introduced by Shalashilin and Child [26,40] and was recently reviewed in [27]. In the following we will briefly recapitulate the so-called coupled coherent state ansatz and its working equations, extending the notation of [27] towards many degrees of freedom.

For a system of $(f+1)$ degrees of freedom as in the previous section, an ansatz for the solution of the time-dependent Schrödinger equation (TDSE) is given in terms of multimode coherent states (CS) of multiplicity M by

$$|\Psi_{\text{CS}}^M(t)\rangle = \sum_{l=1}^M a_l(t) |z_l(t)\rangle, \quad (10)$$

with time-dependent complex coefficients $a_k(t)$ and time-dependent $(f+1)$ -dimensional complex displacement vectors

$$z_l(t) = \frac{\boldsymbol{\gamma}^{1/2} \mathbf{q}_l(t) + i\boldsymbol{\gamma}^{-1/2} \mathbf{p}_l(t)}{\sqrt{2}}, \quad (11)$$

with $\mathbf{q} = (x, y_1, \dots, y_f)$ and $\mathbf{p} = (p_x, p_1, \dots, p_f)$ and diagonal matrix $\boldsymbol{\gamma}$ with entries $\gamma_j = m_j \omega_j$, $j = 0, \dots, f$, where

$\gamma_0 = \gamma_x$, $m_0 = m_x$, and $m_1, \dots, m_f = m$, and we have set $\hbar = 1$.

The $(f+1)$ mode CS are given by an $(f+1)$ -fold tensor product

$$|z_l\rangle = \bigotimes_{j=0}^f |z_{lj}\rangle \quad (12)$$

of normalized one-dimensional CS

$$|z_{lj}\rangle = \exp\left[-\frac{1}{2}|z_{lj}|^2\right] \exp[z_{lj} \hat{a}_j^\dagger] |0_j\rangle, \quad (13)$$

where \hat{a}_j^\dagger is the creation operator acting on the ground state of a suitably chosen j th harmonic oscillator and the CS form an overcomplete and nonorthogonal basis set [41] and are Gaussian wave functions in position space.

To make progress, the Hamiltonian in (5) is to be expressed in terms of the creation and annihilation operators of the harmonic oscillator underlying the CS. In all that follows we will use the normally ordered Hamiltonian, where all appearances of \hat{a}_j^\dagger precede those of \hat{a}_j . Whereas for the bath part of the Hamiltonian, which is harmonic, the task of finding the normally ordered Hamiltonian is trivial, for the quartic bistable system of interest, corresponding to index $j=0$, we give the derivation of the corresponding expression in some detail in Appendix A.

The time evolution of the coefficients and the displacements is now governed by the Dirac-Frenkel variational principle [42,43],

$$\langle \delta \Psi_{\text{CS}}^M | i\partial_t - \hat{H} | \Psi_{\text{CS}}^M \rangle = 0, \quad (14)$$

and we have given the fully variational equations of motion in [44]. In the case that the ansatz (10) is restricted to a single term, i.e., $M=1$, these equations reduce to

$$i\dot{a} = a \left[H_{\text{ord}}(\mathbf{z}^*, \mathbf{z}) - \frac{i}{2} (\dot{\mathbf{z}} \cdot \mathbf{z}^* - \mathbf{z} \cdot \dot{\mathbf{z}}^*) \right], \quad (15)$$

$$i\dot{\mathbf{z}} = \frac{\partial H_{\text{ord}}}{\partial \mathbf{z}^*}. \quad (16)$$

The second of these equations is the complexified Hamilton's equation, and it is given for the present case in Appendix A.

In the CCS method one now reintroduces the multiplicity index and propagates all the coherent state parameters $z_l(t)$ in the ansatz (10) according to the classical equations and keeps the fully variational equations of motion for the coefficients $a_l(t)$ [40], given by

$$i \sum_{l=1}^M \langle z_k(t) | z_l(t) \rangle \dot{a}_l(t) = \sum_{l=1}^M \tilde{H}_{kl}(t) a_l(t), \quad (17)$$

with the time-dependent matrix elements (even in the case of an autonomous Hamiltonian)

$$\tilde{H}_{kl}(t) = \langle z_k(t)|z_l(t)\rangle \left[H_{\text{ord}}(z_k^*, z_l) - \frac{1}{2} \left(z_l(t) \cdot \frac{\partial H_{\text{ord}}(z_l^*, z_l)}{\partial z_l} - \frac{\partial H_{\text{ord}}(z_l^*, z_l)}{\partial z_l^*} \cdot z_l^*(t) \right) - z_k^*(t) \cdot \frac{\partial H_{\text{ord}}(z_l^*, z_l)}{\partial z_l^*} \right], \quad (18)$$

where the elements of the overlap matrix of the multimode CS are given by

$$\begin{aligned} \langle z_k|z_l\rangle &= \prod_{j=0}^f \exp \left[-\frac{1}{2} (|z_{kj}|^2 + |z_{lj}|^2) + z_{kj}^* z_{lj} \right] \\ &= \exp \left[-\frac{1}{2} (|z_l|^2 + |z_k|^2) + z_k^* \cdot z_l \right] \\ &= \exp \left[-(\mathbf{q}_l - \mathbf{q}_k)^T \frac{\mathcal{Y}}{4} (\mathbf{q}_l - \mathbf{q}_k) - (\mathbf{p}_l - \mathbf{p}_k)^T \frac{\mathcal{Y}^{-1}}{4} (\mathbf{p}_l - \mathbf{p}_k) + \frac{i}{2} (\mathbf{p}_l \cdot \mathbf{q}_k - \mathbf{q}_l \cdot \mathbf{p}_k) \right], \end{aligned} \quad (19)$$

which is the product of the corresponding single-mode overlaps. We note that the Klauder phase convention of the corresponding Gaussian wave packets has been used [27].

For the determination of the initial conditions of the trajectories, we are using the pancake sampling idea suggested by Shalashilin and Child [45]. It is the (random) sampling of the initial conditions in the extended (system plus bath) phase space that is believed to help the CCS method cope with the exponential wall, that is usually encountered in grid-based approaches to many-body quantum dynamics.

IV. LONG-TIME DYNAMICS OF THE COUPLED SYSTEM

In the following we present numerical results for the time evolution of the composite system using the method just described to solve the time-dependent Schrödinger equation. In addition, for up to a total of four degrees of freedom (DOF), i.e., $f = 3$, we also corroborated our results by using the split-operator fast Fourier transform (FFT) technique for quantum propagation [46,47]. Our focus will be on the question of whether the coupling to the environmental degrees of freedom, which are all starting in their ground states,

$$\Psi(y_n, 0) = \left(\frac{\gamma_n}{\pi} \right)^{1/4} \exp \left\{ -\frac{\gamma_n}{2} y_n^2 \right\}, \quad (20)$$

will eventually lead to a ‘‘thermalization’’ of the quartic degree towards its ground state (which is depicted in Fig. 1 as the dotted yellow line). We stress that previous treatments of the double-well dynamics using CCS [48] have focused on the description of quantum tunneling, where the initial state is made up of an equal weight superposition of the two lowest energy eigenstates, whereas herein, the initial states consists mostly of state 1 and state 3 (see Table I).

In the following the potential parameters for the double well are $a = 2$ and $b = 1$, and the mass m_x is set equal to unity. The choice of frequencies of the environmental degrees of freedom will be detailed below. All masses of the oscillators are taken to be equal and given by $m = 0.1$.

A. Different numerical measures

As a first measure of the possible deviation of the time-evolved wave function away from the initial state, we use the

autocorrelation function, defined in one dimension (1D) as

$$\begin{aligned} c(t) &= \langle \Psi(0) | \Psi_{\text{CS}}^M(t) \rangle = \sum_{l=1}^M a_l(t) \langle \Psi(0) | z_l(t) \rangle \\ &= \sum_{k,l} a_k^*(0) \langle z_k(0) | z_l(t) \rangle a_l(t). \end{aligned} \quad (21)$$

For a multitude of degrees of freedom, an analogous quantity could be defined by just replacing the scalars z_k, z_l by the corresponding vectors $\mathbf{z}_k, \mathbf{z}_l$, which would, however, not serve our purpose. Our goal is to find an autocorrelation measure, irrespective of the dynamics of the environment. Therefore we first define the probability density of the system degree of freedom by integrating the absolute value squared of the full wave function over all f environmental degrees of freedom,

$$\rho_S(x, t) = \int dy_1 \dots dy_f |\Psi_{\text{CS}}^M(x, y_1, \dots, y_f, t)|^2, \quad (22)$$

to arrive at the probability density of the quartic degree of freedom. This then allows us to calculate the quantity

$$c_S(t) = \int dx \Psi(x, 0) \sqrt{\rho_S(x, t)}, \quad (23)$$

which [if the initial state is real (and positive) as herein] has no phase anymore and is thus the analog of the absolute value of the correlation function of Eq. (21). For the pure quartic (1D) case and the initial state we use, the time evolution of the quantities defined in Eqs. (21) and (23) is similar but not identical. The oscillation period is identical though.

An even more stringent measure to decide if the time-evolved state is approaching the ground state is the energy expectation value, defined by

$$\begin{aligned} \langle E \rangle(t) &= \langle \Psi_{\text{CS}}^M(t) | \hat{H}_{\text{ord}} | \Psi_{\text{CS}}^M(t) \rangle \\ &= \sum_{k,l} a_k^*(t) H_{\text{ord}}(z_k^*, z_l) \langle z_k(t) | z_l(t) \rangle a_l(t). \end{aligned} \quad (24)$$

The different terms in the total Hamiltonian can be disentangled, and their respective contribution to the total energy can be looked at separately. The conservation of the total energy will also serve as a convergence check for the CCS method [49]. In passing, we note that the norm of the total wave function was well conserved in all the numerical

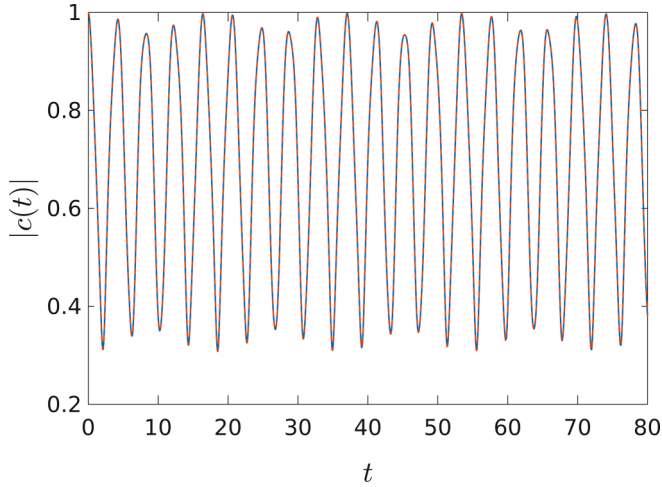


FIG. 2. Absolute value of the autocorrelation function for the 1D system (double well only) from a CCS calculation (solid blue line) and from a split-operator FFT calculation (dashed red line). The two curves coincide to within line thickness.

calculations that we present. This is in contrast to the semi-classical Herman-Kluk case, where often a normalization of the results has to be performed [50]. This is not necessary for CCS.

B. Numerical results

First, we consider the autocorrelation of the initial state at the top of the barrier in the uncoupled 1D case in Fig. 2. For the CCS calculations, a multiplicity of $M = 299$ was enough to converge the result to the converged split-operator FFT result. Because the initial state mainly contains only two eigenstates (see Table I), the local spectrum [51], i.e., the Fourier transform of the autocorrelation, contains just two major peaks. From the figure it can be seen that the absolute value of the autocorrelation correspondingly oscillates back and forth between unity and around 0.3 with a period of around $T = 2\pi/(E_3 - E_1) \approx 4$ in the dimensionless units used. The initial state will thus be revisited frequently in the uncoupled case.

The initial state that will be used in the propagation of the coupled system is the (direct) product of the Gaussian on top of the barrier of the double well, given in Eq. (4), times the ground-state Gaussians of Eq. (20). Before showing the alteration of the results by the coupling of the double well to several oscillators, we have to elaborate on the choice of frequencies of those oscillators, however. This choice will be crucial for the energy flow between the double well and the environment. We again follow the work of DPM [11] and choose the frequencies from the (normalized) density:

$$\rho_f(\omega) = \frac{1}{\omega_{co}} \exp\left\{-\frac{\omega}{\omega_{co}}\right\}, \quad (25)$$

with a parameter ω_{co} to be fixed below, according to

$$\int_0^{\omega_k} d\omega \rho_f(\omega) \stackrel{!}{=} \frac{k}{f_{co}}. \quad (26)$$

TABLE II. Parameters needed for the calculation of the discretized bath frequencies according to Eq. (27) for different values of f .

f	2	3	4	5
ω_{co}	4	4	4	4
f_{co}	10	12	14	16

This leads to the explicit expression

$$\omega_k := -\omega_{co} \ln\left(1 - \frac{k}{f_{co}}\right) \quad k = 1, \dots, f \quad (27)$$

for the frequencies, and we here choose the second parameter $f_{co} > f$, such that extremely high frequencies which would not exchange energy with the system (not shown) are not considered. Other frequency distributions have been used in [34] as well as in [52], while the present one has been found favorable also in multiconfiguration time-dependent Hartree (MCTDH) calculations [53]. Now one could choose the coupling strength between system and environment according to a specific (continuous) spectral distribution, which is usually taken as Ohmic or sub- or super-Ohmic. Here, however, we again adhere to DPM and take equal coupling strengths $g = 0.1$ for all oscillators, just suitably normalized by the total number of environmental degrees of freedom [see remark after Eq. (7)] to make the results for different values of f comparable. In Table II we give the parameters that were used in Eq. (27) for the calculation of the discretized frequencies for different values of f . We note in passing that for the number of oscillators that we will use, and for the present frequencies and couplings (which are renormalized with the square of the number of bath oscillators), there is no transition to monostability of the combination of the bare potential plus the counterterm, mentioned in [39]. In the following, several different quantities will be looked at for increasing numbers of environmental degrees of freedom.

To start with, for the system's "autocorrelation" $c_S(t)$ defined in Eq. (23), we found the results displayed in Fig. 3. For the three-dimensional results ($f = 2$) we used 799 trajectories, whereas for the four-dimensional case ($f = 3$) we used 2999. From Fig. 3 and by comparison to the 1D case displayed in Fig. 2, it can be seen that by the coupling to the environmental degrees of freedom, the oscillation frequency is only marginally increased (as to be expected by comparison to Rabi oscillations in a two-level system), but the oscillation amplitude becomes decisively smaller. Furthermore, a damping of the oscillations for long times can be observed, which becomes the more prominent the higher the number of environmental degrees of freedom. If the quartic subsystem evolves towards the ground state for long times, the expected long-time asymptotic value of the quantity we calculated is $c_S(\infty) = |c_1| \approx 0.8$ (taking the square root of $|c_1|^2$ from Table I). This value is close to the asymptotic average value of the results displayed in Fig. 3.

The most important measure to decide about the propagated density's possible evolution towards the ground state is the energy expectation value. In Fig. 4 the energy expectations for all five degrees of freedom in the case of $f = 4$ as well as

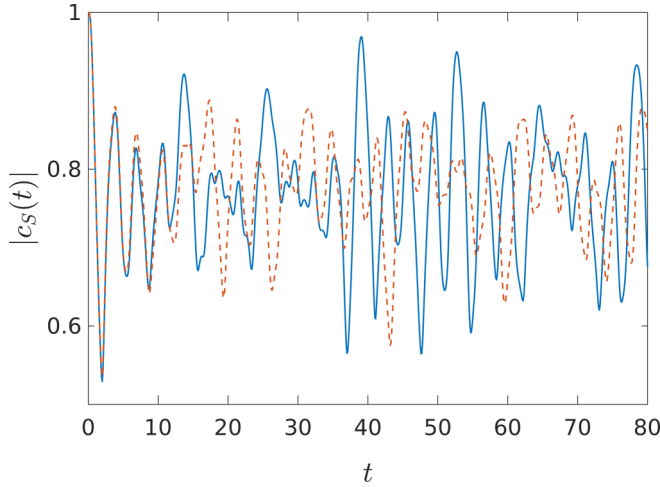


FIG. 3. Absolute value of the autocorrelationlike quantity defined in Eq. (23) from a CCS calculation for different numbers of environmental oscillators: $f = 2$ (solid blue) and $f = 3$ (dashed red).

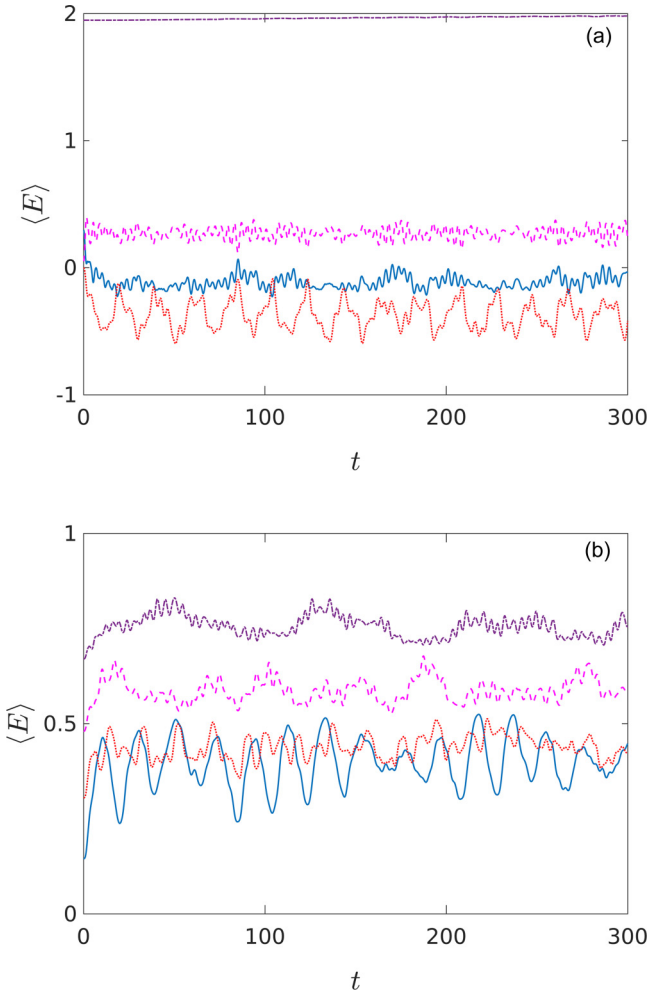


FIG. 4. Different energy expectation values for the case $f = 4$: (a) total energy (dashed-dotted purple), counterterm (dashed magenta), double well (solid blue), coupling term (dotted red), (b) kinetic plus potential energy of the different harmonic degrees of freedom: $\omega_1 = 0.29$ (solid blue), $\omega_2 = 0.61$ (dotted red), $\omega_3 = 0.96$ (dashed magenta), $\omega_4 = 1.34$ (dashed-dotted purple).

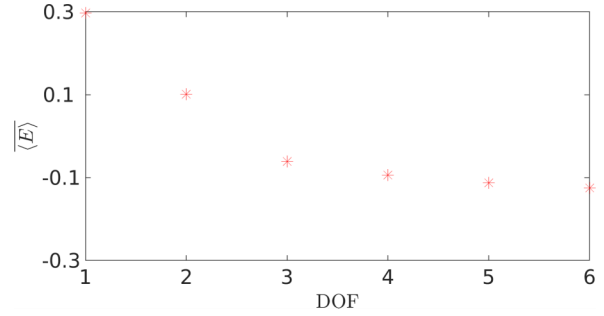


FIG. 5. Long-time average energy of the double well as a function of the total number of degrees of freedom (DOF).

the coupling and the counter term are displayed for times up to $t = 300$, whereby panel (a) contains the total energy, the double-well energy as well as the coupling and the counterterm, and panel (b) contains all the different oscillator energies. The total energy is conserved very well, although a small tendency towards an energy drift is visible [panel (a)]. For the presented results we have used a multiplicity of $M = 5999$, and we did not increase this number because the convergence is becoming exceedingly slow with the number of trajectories and the presented calculation took already several days on a modern computer cluster using several cores. As displayed in panel (b), the different oscillators clearly show an increase in their energy, away from their ground-state value, and the ω_1 oscillator even overtakes the ω_2 oscillator in terms of energy at certain times. We stress that the oscillators' energies never fall below their ground-state energies, as it should be [54]. Furthermore, the oscillator with the highest frequency is still showing appreciable variations in its energy. If even higher frequencies would have been chosen, the energy transfer would start to diminish, however (not shown). We stress that the environment, by consisting of a finite number of degrees of freedom, does heat up, in contrast to the case of infinitely many environmental oscillators described by a continuous spectral density [55]. As shown in panel (a), the counterterm shows high-frequency oscillations with a period similar to the total double-well energy and the interaction energy is large and negative. Most importantly, the total double-well energy shows a clear tendency to decrease below its initial value of 0.3. In addition, for large times the amplitude of oscillation of the double-well energy around its average value is rather small, and we do not observe any revival in the relatively long time span that we display.

This last finding led us to investigate the long-time average value of the double-well energy expectation,

$$\overline{\langle E \rangle} = \frac{1}{T_{\text{tot}}} \int_0^{T_{\text{tot}}} dt \langle E \rangle(t), \quad (28)$$

as a function of the number of environmental oscillators for the relatively long total time of $T_{\text{tot}} = 300$. In the case $f = 1$, the frequency of the single oscillator was $\omega = 0.96$, whereas for $f \in [2, 5]$, the frequencies have been calculated from the parameters given in Table II. As shown in Fig. 5, the average energy of the double-well oscillator indeed decreases as a function of the number of environmental oscillators, indicating a clear trend towards the ground-state energy. In the

Supplemental Material we provide a video of the time evolution of the probability density of the double-well degree of freedom, defined in Eq. (22), for $0 < t < 80$ [56]. This video shows that for long times, the time-evolved density, due to the coupling (in the presented case to three harmonic degrees of freedom), approaches the (static) ground-state density (also displayed in the movie) to a substantial degree.

Finally, it is worthwhile to mention that we have tried different values for the coupling strength g and found (not shown) that larger values lead to too much initial energy from the counterterm (the coupling itself has zero expectation value at $t = 0$) and thus eventually in the system, whereas smaller values of g , due to the small coupling decrease the flow away from the quartic into the harmonic degrees of freedom. So the value $g = 0.1$ that we used was close to optimal if the cooling of the quartic degree of freedom is to be achieved.

V. CONCLUSIONS AND OUTLOOK

By focusing on the toppling pencil model, i.e., an excited initial state on top of the barrier of a symmetric quartic double well, we have investigated if the coupling of the central quartic double well to a finite, environmental bath of harmonic oscillators in their ground states will let the central system evolve towards its ground state. This amounts to the thermalization, i.e., a cooling down to the bath “temperature” (strictly only defined in the thermodynamic limit) of the central system.

By solving the time-dependent Schrödinger equation using the CCS methodology (and also split-operator FFT for small numbers of degrees of freedom), we could show that, indeed, the coupling eventually excites those environmental oscillators, and for the relatively long times investigated, there is no appreciable backflow of energy to the system of interest such that the central degree of freedom loses an appreciable amount of energy, monitored by its long-time average, which we found to be a monotonously decaying function of the number of environmental degrees of freedom. For the largest number $f = 5$ of oscillators that we investigated, the long-time average of the double-well energy decreases from its uncoupled value of 0.3 to -0.125 . This tendency of driving the double well towards lower energy via the environmental coupling was corroborated by an autocorrelation function-like measure, which showed a long-time behavior in accord with the estimate assuming a total transition to the ground state of the quartic degree of freedom. In the light of these results it is worthwhile to note that the variational approach to solving the TDSE is based on a Lagrangian, see, e.g., [40], and the wave-function parameters can be viewed as classical generalized coordinates. There are usually many more of them than in the pure classical approach, where there is only a pair of position and momentum variables per degree of freedom.

We have thus added a further example to the list of continuous-variable systems of interest with (in principle) infinite-dimensional Hilbert space that are coupled to a finite bath and show signs of energetic equilibration. Up to now, the focus in the literature was mainly on spin-chain systems [14,15,24]. The bath, by consisting of a finite number of degrees of freedom, also has a finite heat capacity, in contrast to treatments in terms of reduced density matrices that hinge on continuous spectral densities of the oscillator bath

[55,57]. By (hypothetically) going to the limit of very large f , due to the scaling of the coupling by the inverse of the square root of f , the coupling to the individual oscillators will be diminished and thus also the energy flow, such that the oscillators will stay close to their initial state, which was here one of zero temperature (all oscillators in their ground states). Due to limited computer resources the explicit fully quantum treatment of all degrees of freedom will be difficult in these cases though. Other possible methods to try in the future could be MCTDH [58], matrix product state [20], or different types of semiclassical treatments [27,59].

Furthermore, so far the dynamics studied does not break the symmetry of the initial state of the double well, because the Hamiltonian as well as the initial state of the bath are symmetric under the parity transformation. In the classical mechanics study by Dittrich and Pena Martínez [11], it has been argued that small asymmetries in the initial condition of the bath lead to a preference of the bistable system to end up in one of the wells. It will be a worthwhile endeavor to study such asymmetric initial conditions also in a full quantum time evolution.

ACKNOWLEDGMENTS

The authors would like to thank Professor Marcus Bonanca and Professor Thomas Dittrich for enlightening discussion as well as the International Max Planck Research School for Many Particle Systems in Structured Environments for its support. F.G. would like to thank the Deutsche Forschungsgemeinschaft for financial support under Grant No. GR 1210/8-1.

APPENDIX A: NORMALLY ORDERED HAMILTONIAN AND CLASSICAL EQUATIONS OF MOTION

The Hamilton operator for the quartic double-well potential is given by

$$\hat{H}_S = \hat{T}_S + \hat{V}_S = \frac{\hat{p}_x^2}{2m_x} - \frac{a}{2}\hat{x}^2 + \frac{b}{4}\hat{x}^4. \quad (\text{A1})$$

To make progress, the position and momentum operators are expressed via creation and annihilation operators via

$$\hat{x} = \frac{1}{\sqrt{2}\gamma_x}(\hat{a}_x^\dagger + \hat{a}_x), \quad \hat{p}_x = i\hbar\sqrt{\frac{\gamma_x}{2}}(\hat{a}_x^\dagger - \hat{a}_x). \quad (\text{A2})$$

In the following we set $\hbar = 1$. The subscripts to the creation and annihilation operators denote the respective degree of freedom. Using the fundamental commutation relation

$$[\hat{a}_x, \hat{a}_x^\dagger] = \hat{1}, \quad (\text{A3})$$

the normal ordered form of the kinetic energy operator is found to be

$$\begin{aligned} \hat{T}_S(\hat{a}_x^\dagger, \hat{a}_x) &= \frac{\hat{p}_x^2}{2m_x} = -\frac{\gamma_x}{4m_x}(\hat{a}_x^\dagger - \hat{a}_x)^2 \\ &= -\frac{\gamma_x}{4m_x}[(\hat{a}_x^\dagger)^2 - 2\hat{a}_x^\dagger\hat{a}_x - 1 + \hat{a}_x^2], \end{aligned} \quad (\text{A4})$$

and thus

$$T_S(z_{kx}^*, z_{lx}) = -\frac{\gamma_x}{4m_x}[(z_{kx}^* - z_{lx})^2 - 1] \quad (\text{A5})$$

follows for the CS matrix elements of the normally ordered kinetic energy operator.

Now, for the potential energy operator \hat{V}_S of the system, we have

$$\begin{aligned}\hat{x}^2 &= \frac{1}{2\gamma_x}(\hat{a}_x^\dagger + \hat{a}_x)(\hat{a}_x^\dagger + \hat{a}_x) \\ &= \frac{1}{2\gamma_x}[(\hat{a}_x^\dagger)^2 + 2\hat{a}_x^\dagger\hat{a}_x + 1 + \hat{a}_x^2]\end{aligned}\quad (\text{A6})$$

and

$$\begin{aligned}\hat{x}^4 &= \hat{x}^2\hat{x}^2 = \frac{1}{4\gamma_x^2}[(\hat{a}_x^\dagger)^2 + 2\hat{a}_x^\dagger\hat{a}_x + 1 + \hat{a}_x^2] \\ &\quad \times [(\hat{a}_x^\dagger)^2 + 2\hat{a}_x^\dagger\hat{a}_x + 1 + \hat{a}_x^2] \\ &= \frac{1}{4\gamma_x^2}((\hat{a}_x^\dagger)^4 + \hat{a}_x^\dagger + (\hat{a}_x^\dagger)^2\hat{a}_x^2 + \hat{a}_x^2(\hat{a}_x^\dagger)^2 \\ &\quad + 2(\hat{a}_x^\dagger)^2 + 2\hat{a}_x^2 + 2(\hat{a}_x^\dagger)^3\hat{a}_x + 2\hat{a}_x^\dagger\hat{a}_x^3 + 2\hat{a}_x^2\hat{a}_x^\dagger\hat{a}_x \\ &\quad + 2\hat{a}_x^\dagger\hat{a}_x(\hat{a}_x^\dagger)^2 + 4\hat{a}_x^\dagger\hat{a}_x\hat{a}_x^\dagger\hat{a}_x + 4\hat{a}_x^\dagger\hat{a}_x + 1).\end{aligned}\quad (\text{A7})$$

Using the differential calculus employed in Theorem II on page 142 of [60], the above equation (A7) can be simplified in order to transform all the terms into normal ordered form. To this end one replaces \hat{a} by $z + \partial/\partial z^*$ and \hat{a}^\dagger by z^* and applies the expression to the unit operator to arrive at the matrix elements of the normal form of an operator. \mathcal{N} shall denote the normal ordering operator. Therefore, e.g., from

$$\begin{aligned}\mathcal{N}\left\{\left(z + \frac{\partial}{\partial z^*}\right)^2 (z^*)^2 \cdot 1\right\} &= \mathcal{N}\{z^2(z^*)^2 + 4zz^* + 2\} \\ &= (z^*)^2z^2 + 4z^*z + 2,\end{aligned}\quad (\text{A8})$$

it follows that

$$\hat{a}_x^2(\hat{a}_x^\dagger)^2 = (\hat{a}_x^\dagger)^2\hat{a}_x^2 + 4\hat{a}_x^\dagger\hat{a}_x + 2 \quad (\text{A9})$$

and similarly,

$$\hat{a}_x^2\hat{a}_x^\dagger\hat{a}_x = \hat{a}_x^\dagger\hat{a}_x^3 + 2\hat{a}_x^2, \quad (\text{A10})$$

$$\hat{a}_x^\dagger\hat{a}_x(\hat{a}_x^\dagger)^2 = (\hat{a}_x^\dagger)^3\hat{a}_x + 2(\hat{a}_x^\dagger)^2, \quad (\text{A11})$$

$$\hat{a}_x^\dagger\hat{a}_x\hat{a}_x^\dagger\hat{a}_x = (\hat{a}_x^\dagger)^2\hat{a}_x^2 + \hat{a}_x^\dagger\hat{a}_x, \quad (\text{A12})$$

for all terms that are not normally ordered already. Hence

$$\begin{aligned}\hat{x}^4 &= \frac{1}{4\gamma_x^2}((\hat{a}_x^\dagger)^4 + 4(\hat{a}_x^\dagger)^3\hat{a}_x + 6(\hat{a}_x^\dagger)^2\hat{a}_x^2 + 4\hat{a}_x^\dagger\hat{a}_x^3 + \hat{a}_x^4 \\ &\quad + 6[(\hat{a}_x^\dagger)^2 + 2\hat{a}_x^\dagger\hat{a}_x + \hat{a}_x^2] + 3)\end{aligned}\quad (\text{A13})$$

holds for the normal ordered form of the quartic term in the potential, and the CS matrix elements of the total potential energy for the system are given by

$$\begin{aligned}V_S(z_{kx}^*, z_{lx}) &= -\frac{a}{4\gamma_x}[(z_{kx}^* + z_{lx})^2 + 1] + \frac{b}{16\gamma_x^2} \\ &\quad \times [(z_{kx}^* + z_{lx})^4 + 6(z_{kx}^* + z_{lx})^2 + 3],\end{aligned}\quad (\text{A14})$$

leading to the corresponding Hamiltonian,

$$H_S(z_{kx}^*, z_{lx}) = T_S(z_{kx}^*, z_{lx}) + V_S(z_{kx}^*, z_{lx}), \quad (\text{A15})$$

with the kinetic energy from Eq. (A5). Now the environmental Hamilton operator

$$\begin{aligned}\hat{H}_E &= \sum_{n=1}^f \left(\frac{\hat{p}_n^2}{2m} + \frac{m\omega_n^2}{2}\hat{y}_n^2 \right) \\ &= \sum_{n=1}^f -\frac{\gamma_n}{4m}[(\hat{a}_n^\dagger)^2 - 2\hat{a}_n^\dagger\hat{a}_n - 1 + \hat{a}_n^2] \\ &\quad + \frac{\gamma_n}{4m}[(\hat{a}_n^\dagger)^2 + 2\hat{a}_n^\dagger\hat{a}_n + 1 + \hat{a}_n^2] \\ &= \sum_{n=1}^f \omega_n \left(\hat{a}_n^\dagger\hat{a}_n + \frac{1}{2} \right)\end{aligned}\quad (\text{A16})$$

is already normal ordered, leading to the matrix elements

$$H_E(z_{ky_1}^*, \dots, z_{ky_n}^*, z_{ly_1}, \dots, z_{ly_n}) = \sum_{n=1}^f \omega_n \left(z_{ky_n}^* z_{ly_n} + \frac{1}{2} \right). \quad (\text{A17})$$

The same holds true for the interaction Hamilton operator

$$\hat{H}_{SE} = -\hat{x} \sum_{n=1}^f g_n \hat{y}_n, \quad (\text{A18})$$

leading to

$$\begin{aligned}H_{SE}(z_{kx}^*, z_{ky_1}^*, \dots, z_{ky_n}^*, z_{lx}, z_{ly_1}, \dots, z_{ly_n}) \\ = -\frac{(z_{kx}^* + z_{lx})}{2\sqrt{\gamma_x}} \sum_{n=1}^f \frac{g_n}{\sqrt{\gamma_n}} (z_{ky_n}^* + z_{ly_n}).\end{aligned}\quad (\text{A19})$$

Finally, the counterterm operator

$$\hat{V}_C = \hat{x}^2 \sum_{n=1}^f \frac{g_n^2}{2m\omega_n^2} \quad (\text{A20})$$

is just quadratic and leads to

$$V_C(z_{kx}^*, z_{lx}) = [(z_{kx}^* + z_{lx})^2 + 1] \sum_{n=1}^f \frac{g_n^2}{4m\omega_n^2\gamma_x}. \quad (\text{A21})$$

Therefore the total normal ordered Hamiltonian is given by the sum of all the terms in Eqs. (A15), (A17), (A19), and (A21) as

$$\begin{aligned}H_{\text{ord}}(z_k^*, z_l) &= -\frac{\gamma_x}{4m_x}[(z_{kx}^* - z_{lx})^2 - 1] - \frac{a}{4\gamma_x}[(z_{kx}^* + z_{lx})^2 + 1] \\ &\quad + \frac{b}{16\gamma_x^2}[(z_{kx}^* + z_{lx})^4 + 6(z_{kx}^* + z_{lx})^2 + 3] \\ &\quad + \sum_{n=1}^f \omega_n \left(z_{ky_n}^* z_{ly_n} + \frac{1}{2} \right) - \frac{(z_{kx}^* + z_{lx})}{2\sqrt{\gamma_x}} \sum_{n=1}^f \frac{g_n}{\sqrt{\gamma_n}} \\ &\quad \times (z_{ky_n}^* + z_{ly_n}) + [(z_{kx}^* + z_{lx})^2 + 1] \sum_{n=1}^f \frac{g_n^2}{4m\omega_n^2\gamma_x}.\end{aligned}\quad (\text{A22})$$

The complexified classical equation of motion for the displacements z_x of the quartic degree of freedom is given by

$$i\dot{z}_x = \frac{\partial H_{\text{ord}}}{\partial z_x^*} = -\frac{\gamma_x}{2m_x}(z_x^* - z_x) + \frac{b}{4\gamma_x^2}(z_x^* + z_x)^3 - \sum_{n=1}^f \frac{g_n}{2\sqrt{\gamma_x\gamma_n}}(z_{y_n}^* + z_{y_n}) + \frac{(z_x^* + z_x)}{2\gamma_x} \left[\sum_{n=1}^f \frac{g_n^2}{m\omega_n^2} - a + \frac{3b}{2\gamma_x} \right]. \quad (\text{A23})$$

The equations of motion for the displacements z_{y_n} of the harmonic (environmental) degrees of freedom are

$$i\dot{z}_{y_n} = \frac{\partial H_{\text{ord}}}{\partial z_{y_n}^*} = \omega_n z_{y_n} - \frac{g_n}{2\sqrt{\gamma_x\gamma_{y_n}}}(z_x^* + z_x). \quad (\text{A24})$$

The equations of motion for the coefficients in the CS expansion are given in (17).

-
- [1] E. Fermi, J. Pasta, and S. Ulam, in *Collected Papers of Enrico Fermi*, edited by E. Segré (University of Chicago Press, Chicago, IL, 1965).
- [2] J. Ford, *Phys. Rep.* **213**, 271 (1992).
- [3] M. V. Berry and J. M. Robbins, *Proc. R. Soc. London A* **442**, 659 (1993).
- [4] C. Jarzynski, *Phys. Rev. Lett.* **74**, 2937 (1995).
- [5] M. V. S. Bonanca and M. A. M. de Aguiar, *Physica A* **365**, 333 (2006).
- [6] J. Rosa and M. W. Beims, *Phys. Rev. E* **78**, 031126 (2008).
- [7] S. Smith and R. Onofrio, *Eur. Phys. J. B* **61**, 271 (2008).
- [8] M. A. Marchiori and M. A. M. de Aguiar, *Phys. Rev. E* **83**, 061112 (2011).
- [9] M. A. Marchiori, R. Fariello, and M. A. M. de Aguiar, *Phys. Rev. E* **85**, 041119 (2012).
- [10] F. Jin, T. Neuhaus, K. Michielsen, S. Miyashita, M. A. Novotny, M. I. Katsnelson, and H. De Raedt, *New J. Phys.* **15**, 033009 (2013).
- [11] T. Dittrich and S. Pena Martínez, *Entropy* **22**, 1046 (2020).
- [12] M. Buchholz, C.-M. Goletz, F. Grossmann, B. Schmidt, J. Heyda, and P. Jungwirth, *J. Phys. Chem. A* **116**, 11199 (2012).
- [13] J. G. Cosme and O. Fialko, *Phys. Rev. A* **90**, 053602 (2014).
- [14] R. V. Jensen and R. Shankar, *Phys. Rev. Lett.* **54**, 1879 (1985).
- [15] J. Gemmer, M. Michel, and G. Mahler, *Quantum Thermodynamics: Emergence of Thermodynamic Behavior Within Composite Quantum Systems*, Lecture Notes in Physics, Vol. 784 (Springer Verlag, Berlin, 2009).
- [16] T. Klamroth and M. Nest, *Phys. Chem. Chem. Phys.* **11**, 349 (2009).
- [17] M. Galiceanu, M. W. Beims, and W. Strunz, *Physica A* **415**, 294 (2014).
- [18] C. Khripkov, D. Cohen, and A. Vardi, *J. Phys. Chem. A* **120**, 3136 (2016).
- [19] P. Reimann, *Nat. Commun.* **7**, 10821 (2016).
- [20] R. Borrelli and M. F. Gelin, *New J. Phys.* **22**, 123002 (2020).
- [21] L. D'Alessio, Y. Kafri, A. Polkovnikov, and M. Rigol, *Adv. Phys.* **65**, 239 (2016).
- [22] J. M. Deutsch, *Rep. Prog. Phys.* **81**, 082001 (2018).
- [23] M. Buchholz, F. Grossmann, and M. Ceotto, *J. Chem. Phys.* **148**, 114107 (2018).
- [24] D. Hetterich, M. Fuchs, and B. Trauzettel, *Phys. Rev. B* **92**, 155314 (2015).
- [25] T. Dittrich, F. Grossmann, P. Hänggi, B. Oelschlägel, and R. Utermann, in *Stochasticity and Quantum Chaos*, edited by Z. Haba, W. Cegla, and L. Jakóbczyk (Kluwer, Dordrecht, 1995), pp. 39–55.
- [26] D. V. Shalashilin and M. S. Child, *J. Chem. Phys.* **113**, 10028 (2000).
- [27] M. Werther, S. Loho Choudhury, and F. Grossmann, *Int. Rev. Phys. Chem.* **40**, 81 (2021).
- [28] F. Hund, *Z. Phys.* **43**, 805 (1927).
- [29] J. Kurkijärvi, *Phys. Rev. B* **6**, 832 (1972).
- [30] E. Kierig, U. Schnorrberger, A. Schietinger, J. Tomkovic, and M. K. Oberthaler, *Phys. Rev. Lett.* **100**, 190405 (2008).
- [31] L. E. Reichl, *The Transition to Chaos: Conservative Classical Systems and Quantum Manifestations*, 2nd ed. (Springer, New York, 2004).
- [32] A. J. Bray and M. A. Moore, *Phys. Rev. Lett.* **49**, 1545 (1982).
- [33] A. J. Leggett, S. Chakravarty, A. T. Dorsey, M. P. A. Fisher, A. Garg, and W. Zwerger, *Rev. Mod. Phys.* **59**, 1 (1987).
- [34] R. Hartmann, M. Werther, F. Grossmann, and W. T. Strunz, *J. Chem. Phys.* **150**, 234105 (2019).
- [35] F. Großmann and P. Hänggi, *Europhys. Lett.* **18**, 571 (1992).
- [36] M. Grifoni and P. Hänggi, *Phys. Rep.* **304**, 229 (1998).
- [37] G.-L. Ingold, *Coherent Evolution in Noisy Environments*, edited by A. Buchleitner and K. Hornberger, Lecture Notes in Physics, Vol. 611 (Springer, Berlin, 2002), pp. 1–53.
- [38] A. O. Caldeira and A. J. Leggett, *Ann. Phys.* **149**, 374 (1983).
- [39] S. Choi, R. Onofrio, and B. Sundaram, *Phys. Rev. E* **92**, 042907 (2015).
- [40] D. V. Shalashilin and I. Burghardt, *J. Chem. Phys.* **129**, 084104 (2008).
- [41] V. Bargmann, P. Butera, L. Girardello, and J. R. Klauder, *Rep. Math. Phys.* **2**, 221 (1971).
- [42] P. A. M. Dirac, *Math. Proc. Cambridge Philos. Soc.* **26**, 376 (1930).
- [43] J. Frenkel, *Wave Mechanics: Advanced General Theory*, 1st ed. (Oxford University Press, Oxford, 1934).
- [44] M. Werther and F. Grossmann, *Phys. Rev. B* **101**, 174315 (2020).
- [45] D. V. Shalashilin and M. S. Child, *J. Chem. Phys.* **128**, 054102 (2008).
- [46] M. D. Feit, J. A. Fleck, and A. Steiger, *J. Comput. Phys.* **47**, 412 (1982).
- [47] We note that the number of grid points in the x direction needed for convergence was just 32 (for the grid extension $x \in [-3.5, 3.5]$) and thus much less than in the finite-difference approach in Sec. II A. Furthermore, the number of grid points we took for the harmonic degrees varied between 128 for the low-frequency oscillators and 64 for the high-frequency ones. The time step for propagation was $\Delta t = 0.01$.

- [48] P. A. J. Sherratt, D. V. Shalashilin, and M. S. Child, *Chem. Phys.* **322**, 127 (2006).
- [49] S. Habershon, *J. Chem. Phys.* **136**, 014109 (2012).
- [50] M. Thoss and G. Stock, *Phys. Rev. A* **59**, 64 (1999).
- [51] F. Grossmann, *Theoretical Femtosecond Physics: Atoms and Molecules in Strong Laser Fields*, 3rd ed. (Springer International Publishing AG, Cham, Switzerland, 2018).
- [52] C.-M. Goletz, W. Koch, and F. Grossmann, *Chem. Phys.* **375**, 227 (2010).
- [53] H. Wang and M. Thoss, *New J. Phys.* **10**, 115005 (2008).
- [54] M. Buchholz, E. Fallacara, F. Gottwald, M. Ceotto, F. Grossmann, and S. D. Ivanov, *Chem. Phys.* **515**, 231 (2018).
- [55] Y. Tanimura, *J. Chem. Phys.* **153**, 020901 (2020).
- [56] See Supplemental Material at <http://link.aps.org/supplemental/10.1103/PhysRevA.105.022201> for a video showing the evolution of the 1D probability density $\rho_S(x, t)$ from the coupled dynamics with $f = 3$ harmonic oscillators is displayed on top of the ground-state density (static blue line) of the unperturbed double-well potential in the interval $0 < t < 80$.
- [57] U. Weiss, *Quantum Dissipative Systems*, 3rd ed. (World Scientific, Singapore, 2008).
- [58] M. H. Beck, A. Jäckle, G. A. Worth, and H.-D. Meyer, *Phys. Rep.* **324**, 1 (2000).
- [59] F. Grossmann, *J. Chem. Phys.* **125**, 014111 (2006).
- [60] W. H. Louisell, *Quantum Statistical Properties of Radiation* (Wiley, New York, 1990).